

## Chapter 12

# IMAGING CARBON NANOTUBES *IN VIVO*: A VIGNETTE OF IMAGING MODALITIES AT THE NANOSCALE

**Khuloud T. Al-Jamal<sup>a</sup> and Kostas Kostarelos<sup>b</sup>**

<sup>a</sup> *Institute of Pharmaceutical Science, King's College London, Franklin-Wilkins Building, London SE1 9NH, UK*

<sup>b</sup> *Nanomedicine Lab, Centre for Drug Delivery Research, The School of Pharmacy, University of London, 29–39 Brunswick Square, London WC1N 1AX, UK*

kostas.kostarelos@pharmacy.ac.uk

### 12.1 INTRODUCTION

Nanotechnology is an interdisciplinary research effort bridging many scientific fields from physics and chemistry to engineering, biology, and medicine. The result of such interconnections is holding great potential for the early detection, diagnosis, and personalized treatment of disease. The nanoscale range at which nanosystems operate, i.e., one-thousandth smaller than a human cell, can offer facile transport across the human body and intracellular interactions with many cell components that would otherwise be inaccessible. Imaging for early detection and diagnosis of diseases using newly emerged nanoparticles such as quantum dots (QDs) [21], carbon nanotubes (CNTs) [19], nanoshells [10], paramagnetic nanoparticles [34], and others [6, 9] have been an area of interest over the last few years.

Carbon nanotubes are a type of nanomaterial that offers unique intrinsic properties that make them very interesting candidates as imaging contrast agents. Their identification in the early 1990s [12] and their further biomedical development [18] opened a new era in the development of novel delivery systems for therapeutics and diagnostics. Carbon nanotubes are mainly classified as single-walled (SWNTs)

---

*Nanoimaging*

Edited by Beth Goins and William Phillips

Copyright © 2011 by Pan Stanford Publishing Pte. Ltd.

www.panstanford.com

or multiwalled (MWNTs) according to the number of concentric layers of graphitic sheets rolled into cylindrical structures. The high aspect ratio of CNT offers great advantages over other nanoparticle types, since the high surface area provides multiple attachment sites for drugs, targeting ligands, and imaging probes. Advancements achieved in filling CNT with small molecules or other nanomaterials also indicate an opportunity to use them as imaging probes *in vivo* [11, 30, 35]. One of the main disadvantages of CNT is their hydrophobicity, so advances in solubilization and dispersion methodologies, including chemical functionalization of the CNT surface [4] or coating with amphiphilic molecules such as PEGylated phospholipids or polymers [13], have been an essential breakthrough to allow exploitation of the biomedical applications of CNT. Recently, successful studies in our laboratories as well as others have reported that CNT can translocate into cells using several analytical techniques, including optical microscopy, micro-Raman spectroscopy, single-particle tracking (SPT), transmission electron microscopy (TEM), flow cytometry, and fluorescence microscopy. Moreover, proof-of-concept studies have established that CNT can act as delivery systems for drugs (methotrexate, amphotericin) [26, 37], antigens, and genes (plasmid DNA, siRNA) [14, 32] into prokaryotic and mammalian cells with minimal cytotoxicity both *in vitro* [3, 5] and *in vivo* [2, 27, 40]. This indeed allows for using CNTs not only as multimodal imaging probes but also as theranostic devices.

In this chapter, we will specifically focus on the applications of CNTs as imaging contrast agents *in vivo*, with an overview on the different imaging techniques available for CNT imaging, and also discuss their limitations. Although the studies discussed here all fall within the preclinical settings, the unique properties of CNTs and the ongoing efforts on improving their biocompatibility, in addition to advances in the imaging field, hold a great promise for clinical applications in the future. Imaging modalities that will be discussed here and that have successfully tested CNTs as imaging contrast agents preclinically *in vivo* include single photon emission computed tomography (SPECT), positron emission tomography (PET), magnetic resonance imaging (MRI), optical fluorescence, and ultrasound. The list of the techniques and the comprehensive list of relevant studies are shown in Table 12.1.

## 12.2 MODALITIES FOR *IN VIVO* IMAGING

CNTs developed as imaging contrast agents can be classified on the basis of their surface properties into three main types: (i) pristine CNTs (pCNTs), (ii) coated (noncovalently surface modified) CNTs, and (iii) covalently modified CNTs. A schematic showing the type of modification and the modalities used to image CNT-based contrast agents is shown in Fig. 12.1.

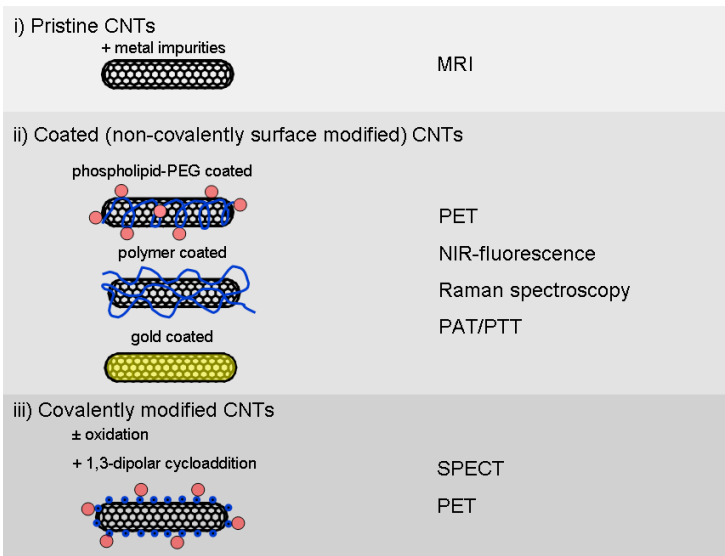


**Figure 12.1** Types of CNT studied as imaging contrast agents *in vivo* and the imaging techniques involved.

### 12.2.1 Single Photon Emission Computed Tomography

SPECT allows whole-body dynamic imaging of the same animal repeatedly, and therefore it is suitable to monitor and study changes in tissue distribution following administration within a timeframe determined by the half-life of the radioisotope used. Conventional gamma counting can be used in parallel with imaging studies to allow more accurate quantification of the biodistribution profile. Our laboratory has collaborated with others to report the first study of CNTs used in dynamic imaging of living small animals using SPECT [20]. The CNT surface was chemically functionalized by 1,3-dipolar cyclo-addition reaction without prior oxidation (MWNT-NH<sub>3</sub><sup>+</sup>), where the ammonium functional groups were covalently conjugated to the chelating molecule diethylenetriaminepentaacetic (DTPA) and labeled with the gamma emitter indium-111 (<sup>111</sup>In) for imaging purposes ( $t_{1/2} = 2.81$  days). The radiolabeled CNTs were injected intravenously via tail vein and showed kidney clearance with no radioactivity left in the body within the first 24 hours. SPECT showed that the nanotubes enter the systemic blood circulation and within 5 minutes begin to permeate through the renal glomerular filtration system into the bladder (Fig. 12.2). Clearance of imaging agents can have an impact on their toxicological profile, and fast clearance makes their use greatly favorable. We have also previously reported the *in vivo* biodistribution profile of SWNTs chemically functionalized by the same method as reported with *f*-MWNT [31]. The same biodistribution profile of MWNT-NH<sub>3</sub><sup>+</sup> was observed suggesting the suitability of both functionalized SWNTs and MWNTs for SPECT imaging.

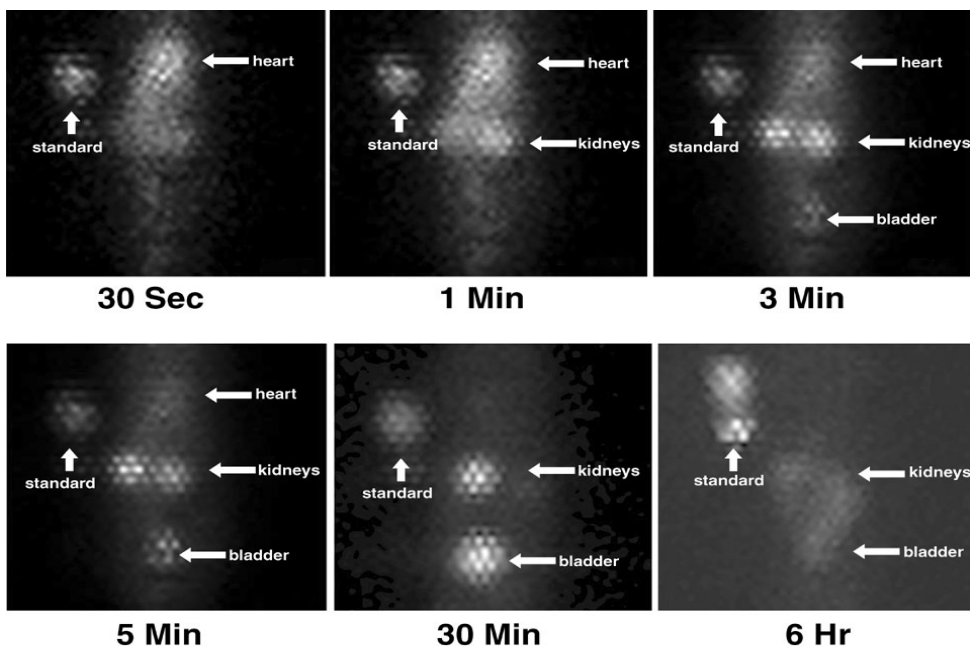


**Figure 12.2** Serial single-photon planar images of  $^{111}\text{In}$  radiolabeled functionalized MWNTs administered intravenously to a normal rat. Radiolabeled nanotubes are visualized in the blood pool of the heart at 30 seconds, but very rapidly at 1 minute the CNTs begin to accumulate in the kidneys and move into the bladder by 3 minutes. By 6 hours, the majority of the activity has cleared the body, as can be observed by comparing the rat image with the image standard. The pixilated appearance of the image is due to the large size of the camera collimator holes required for imaging high-energy  $^{111}\text{In}$  photons. (Images obtained during collaboration with Drs. B. Goins and W. Phillips, University of Texas Health Science Center, San Antonio. [20])

### 12.2.2 Positron Emission Tomography

The first PET study, described by McDevitt *et al.* [24], used shortened (carboxylated) ammonium functionalized SWNT conjugated with the chelating molecule 1,4,7,10-tetraazacyclo-dodecane-1,4,7,10-tetraacetic acid (DOTA) for labeling with the short half-lived positron-emitting isotope yttrium-86 ( $^{86}\text{Y}$ ) ( $t_{1/2} = 14.7$  hours) for PET imaging. The labeled CNTs were imaged, and the biodistribution profile was concluded. The administration was via the intraperitoneal (IP) or via the intravenous (IV) route through the retro-orbital sinus in athymic nude mice. PET imaging showed clear signals in the liver, spleen, and kidney, primarily the renal cortex. The spleen and the liver showed less uptake after IP administration compared with IV administration. Within 24 hours, kidney clearance was observed, while liver and spleen signals remained almost unchanged. The blood clearance profile indicated rapid clearance from the blood compartment with no radioactivity detected at 3 hours. PET imaging

was conclusive on the biodistribution profile of the contrast agent at early time points after administration restricted by the half-life of yttrium. However, deep tissue imaging was possible with excellent penetration capacity of the radionuclide signal. Although no active targeting was employed in this PET imaging study, a previous study performed by the same group had shown that the same CNT construct used in PET imaging was able to target a disseminated (bone marrow) human lymphoma murine xenograft model after chemical conjugation of the monoclonal antibody Rituximab onto the CNT surface. Rituximab targeted the CD20 epitope on human Burkitt lymphoma cells for radionuclide targeting to the cells. In conclusion, the work by McDevitt *et al.* [24, 25] using shortened ammonium functionalized SWNTs (<100 nm in length) conjugated to DOTA showed rapid clearance of both targeted and nontargeted radiolabeled CNT constructs from the blood stream. However, conjugation of Rituximab antibody to the DOTA-SWNT dramatically altered the biodistribution, with lower kidney and higher liver accumulation. The differential organ accumulation observed here could be due to the different hydrophobicity/bundling of the DOPA-functionalized SWNTs, as has been reported by these authors [24]. This means that by appropriately designing CNT-based diagnostics and therapeutic systems, one may be able to establish platforms with altered lung, liver, and spleen accumulation versus kidney clearance. This is again a criterion necessary for selective organ imaging.

Another *in vivo* PET study was performed by Dai and colleagues [22], who imaged SWNTs coated with phospholipids bearing polyethylene glycol chains on their polar headgroups. The radiolabel used was copper-64 ( $^{64}\text{Cu}$ ) with a  $t_{1/2} = 12.7$  hours, attached to the PEG chain chemically conjugated to DOTA at their distal ends. RGD peptides were also conjugated to the radiolabeled SWNTs to serve as targeting ligands specific for integrin-positive tumors via RGD- $\alpha_v\beta_3$  integrin binding. The length of PEG was changed, and two molecular weights were used: 2000 Da and 5400 Da. The results reported showed a prolonged blood circulation profile and low uptake by the reticuloendothelial system (RES) at early time points following administration. Tumor targeting was also achieved by conjugation of RGD to the PEG termini coating the CNTs after tail vein administration in mice bearing  $\alpha_v\beta_3$  integrin-positive U87MG subcutaneous tumors. SWNT coated with both lipopolymer types eventually deposited prominently in the liver and the spleen, with lower uptake in these organs of the SWNT-PEG5400 compared with SWNT-PEG2000. SWNT-PL-PEG5400 also exhibited longer blood circulation time ( $t_{1/2} = 0.5$  hour). Other organs such as solid tumor, muscle, bone, and skin showed low uptake. RGD-functionalized SWNT-PL-PEG2000 showed only slight increase in tumor uptake compared with nontargeted SWNT-PL-PEG2000. However, SWNT-PL-PEG5400-RGD exhibited higher tumor uptake (>10% ID/g tissue) compared with nontargeted SWNT-PL-PEG5400 (3–4% ID/g tissue), with a peak at 6 hours and leveling off at 20 hours post-injection. The PET imaging results reported in this study were confirmed semiquantitatively using *ex vivo* Raman spectroscopy.

### 12.2.3 Near-Infrared Fluorescence

One of the major drawbacks of optical imaging in living animals is the poor tissue penetration and intense scattering of light. The near-infrared (NIR) photoluminescence intrinsic to only individualized semiconducting SWNTs, mostly in the infrared-A (IR-A, 1–1.4  $\mu\text{m}$ ) region, has made them promising as novel NIR fluorescence contrast agents. In preclinical small animal imaging studies, low autofluorescence and deep tissue penetration in the NIR region beyond 1 mm can be achieved using such probes.

NIR imaging of SWNTs in live animals, however, remains challenging. The first study that employed the intrinsic NIR fluorescence of SWNTs to measure the blood elimination kinetics in rabbits and to identify the organs in which they concentrate was performed by Cherukuri *et al.* [7]. That study demonstrated that pristine SWNTs, dispersed by coating of the block copolymer Pluronic F108, can be detected through their intrinsic NIR after jugular vein administration. NIR signals were detected in blood samples and excised tissues. Blood circulation half-life was 0.1 hour, and after 2 hours most of the dose was detected in the liver. Although this technique does not require complex modification of the SWNTs as in linking or conjugation chemistries of fluorophores and radioisotopes, preparation of SWNTs to render them water dispersible and biocompatible have been shown to affect their quantum yield, thereby making the use of this technique limited to *in vitro* imaging or superficial *in vivo* imaging of pristine SWNTs [36]. The main limitation of this technique is the low quantum efficiency of SWNTs and the diffraction to resolution. Also, quantitative data are difficult to obtain using this technique. Recently, Welsher *et al.* reported that the method of SWNT coating is essential and dictates the sensitivity levels of this imaging technique [36]. The study has shown nude mice injected with two types of coated SWNTs: (i) direct SWNTs coated with phospholipid–PEG and (ii) SWNTs solubilized with sodium cholate first, followed by surfactant exchange to form phospholipid–PEG-coated nanotubes. The exchange procedure was found to improve the sensitivity of detection of signals by 15 times, allowing for deep tissue penetration and low autofluorescence background for imaging of tumor vessels beneath thick skin using high-resolution intravital microscopy, with an InGaAs camera in the 1–1.7 mm spectral range. Authors have attributed this to less damage to the nanotubes that improved the quantum yield during sonication.

### 12.2.4 Raman Spectroscopy

The first preclinical study to analyze CNTs deposited in tissue samples by Raman spectroscopy *ex vivo* was performed by Liu *et al.* [22] using SWNTs coated with PEGylated lipids. Such analytical tool was employed to confirm the tissue distribution results obtained by PET imaging of physically adsorbed PEG (2000 and 5400 Da) onto the surface of SWNTs targeted with RGD peptide. Confirmation of the presence of SWNTs (for an injected dose of 0.5 mg/kg) in liver and tumor tissues by using the

intrinsic optical properties of SWNTs was offered on the basis of the strong resonance Raman bands, including the G band at  $\sim 1580\text{ cm}^{-1}$ , which is characteristic of graphitic carbon. In a subsequent study [23] the intrinsic Raman scattering intensity of SWNTs was used to quantify the concentration of nanotubes in blood and mice organs *ex vivo* (tissue lysates). It was shown that the longer and more branched the PEG chains, the longer the blood circulation time and lower the liver and spleen uptake. Also, slow but persistent decrease in the SWNT Raman signal suggested clearance of SWNTs through the biliary route and kidney. SWNT Raman signals were found in the intestine, feces, kidney, and bladder.

Kang *et al.* [16] have studied the biodistribution of shortened SWNTs (50–200 nm in length and 1–3 nm in diameter) coated with chitosan or chitosan-Alexa Fluor 488, injected via the tail vein of nude mice at a dose of 5 or 20  $\mu\text{g}/\text{animal}$ . Tissue uptake was monitored at 0.5 hour to 24 hours after administration by fluorescence microscopy and Raman spectroscopy. The liver was found to have the highest nanotube uptake, with a maximum CNT accumulation at 3 hours followed by relatively high levels in the spleen and kidney. Raman signals in other organs were low ( $<5\%$  ID/g). The sensitivity threshold was 3–4.5% ID/g tissue at 20  $\mu\text{g}$  dose. Blood circulation half-life was 3–4 hours. No reduction in liver uptake was observed up to 24 hours. Similarly, rapid uptake and slow clearance was found in the spleen, whereas the kidney showed faster clearance of SWNT compared with the liver and spleen, where almost 50% dose detected in the kidney at 3 hours was excreted out 24 hours after injection. No Raman signals were detected in urine and feces, and this was attributed to the low sensitivity of the technique.

Raman spectroscopy offers the advantage of long-term tracking of SWNT in organs up to several months and offers high sensitivity in the case of noncovalent coating of SWNTs. On the other hand, disadvantages include (i) limited detection sensitivity, with minimum detection levels reported at 0.04  $\mu\text{g}/\text{ml}$  in blood (0.2%ID/g) and 0.2  $\mu\text{g}/\text{ml}$  in other tissues (1%ID/g) [23]; (ii) unsuitability for chemically functionalized SWNTs that generally induces defects on the nanotube backbone, thereby dramatically compromising signal intensity; (iii) and restriction to *ex vivo* (blood and dissected tissue) sample analyses. However, in a recent study performed by Zavaleta *et al.* [39], SWNTs coated with lipid-PEG5000-RGD and injected intravenously in mice bearing U87MG  $\alpha_v\beta_3$  integrin-positive subcutaneous tumors, it was reported that Raman spectroscopy can also be used successfully for noninvasive tissue imaging of the superficial tumors. Optimization of the technique is still required to improve the depth and accuracy of the imaging (maximum depth achieved was 2 mm), with more quantification data still needed to correlate with *ex vivo* analyses.

Raman spectroscopy has been used to study the tissue distribution and *in vivo* stability of covalently PEGylated SWNT (PEG<sub>1500</sub>-SWNT) after systemic administration in correlation with photo-bioluminescence measurements. De-PEGylation from the SWNTs was reported taking place in the liver at 4–8 weeks after injection, but not in

the spleen [38]. Generally, pristine and acid-treated SWNTs exhibit a characteristic Raman spectrum with a distinct G-band peak at around  $1590\text{ cm}^{-1}$ . However, this peak is less intense upon covalent functionalization, as in the case of PEGylated SWNT studied in the report by Yang *et al.*, leading to significant interference and the G-band signals becoming barely detectible. Therefore, detection sensitivity is a serious limitation of this imaging technique, particularly when it comes to chemically functionalized CNTs.

### 12.2.5 Magnetic Resonance Imaging

MRI detects the interaction of water protons with each other and with the surrounding media. Different tissues have different relaxation times, and MRI contrast agents can enhance the relaxation time further, which is represented by the shortening of either  $T_1$  (longitudinal) or  $T_2$  (transverse) relaxation time. Super-paramagnetic iron oxides (SPIOs) affect the  $T_2$  relaxation time more significantly than  $T_1$ , whereas gadolinium chelates predominantly affect  $T_1$ . Although MRI offers great resolution to reveal the spatial anatomical structure, it suffers from inherently low sensitivity. This can be improved by the use of contrast agents, prolonging the scanning time or increasing the strength of the magnetic field. CNTs have shown potential as MRI contrast agents, where  $\text{Gd}^{+3}$ -grafted SWNTs (gadonanotubes) have been reported to have an MRI efficacy 40 times greater than other  $\text{Gd}^{+3}$ -based contrast agents [33]. In addition, the confinement of  $\text{Gd}^{+3}$  ions onto ultrashort SWNT has made them super-paramagnetic. They have also shown pH-dependent response, which can be useful in imaging the acidic environment of tumors. However, no *in vivo* studies have been performed using such gadonanotubes to illustrate their imaging efficacy in the biological environment. A noninvasive follow-up study would be beneficial to evaluate the biodistribution and effect of nanotube tissue deposition after exposure directly *in vivo*.

The only study that has shown *in vivo* MRI capacity of SWNTs performed today [1] combined He-3 and H-1 magnetic resonance in a rat model to evaluate the biodistribution and biological impact of raw single-wall (raw SWNT) and superpurified (SP SWNT) nanotubes. The effects induced by metal impurities in the intrapulmonary instilled raw SWNT samples induced a significant decrease in magnetic field homogeneity detected in He-3 MRI acquired under spontaneous breathing conditions using a multi-echo radial sequence. H-1 MRI allowed detection of intravenously injected raw SWNTs in the spleen and kidneys using a gradient echo sequence sensitive to changes of relaxation time values. Histological analysis confirmed the absence of SWNTs in organs other than the lung following intrapulmonary instillation of the material. This study concluded that hyperpolarized He-3 can be used for the investigation of CNT pulmonary biodistribution, while standard H-1 MRI may best be utilized for imaging nanotube dispersions following systemic administration.

### 12.2.6 Photo-acoustic Tomography

PAT is a cross-sectional imaging technique based on the photo-acoustic effect of nanomaterials. PAT offers higher spatial resolution and better tissue penetration than conventional optical imaging techniques. In a recent study, SWNTs coated with lipid-PEG-RGD molecules were used as a contrast agent for PAT in U87MG tumor models in living mice [8]. Intravenous administration of this nanotube conjugate to tumor-bearing animals showed eight times photo-acoustic signal enhancement in the tumor compared with mice injected with nontargeted (no RGD) SWNTs. Results were confirmed by *ex vivo* Raman spectroscopy; however, the SWNTs studied lacked sensitivity, since at an SWNT concentration of 50 nM the photo-acoustic signal produced was equivalent to background tissue, and only at higher nanotube concentrations a signal could be detected *in vivo*.

CNTs have also been shown to be promising photothermal contrast agents [15, 29], even though *in vivo* applications have been limited by the relatively low absorption displayed by nanotubes at NIR wavelengths and the concerns over toxicity. Kim *et al.* [17] have recently deposited a thin layer of gold (4–8 nm thick) around shortened CNTs (100 nm in length and 1.5–2 nm in diameter) forming what they termed *golden carbon nanotubes* (GNTs). The gold layer acted as an NIR absorption enhancer and could modulate their toxicity. GNTs have shown the capacity to act as photoacoustic and photothermal contrast agents, exhibiting enhanced near-infrared contrast (approximately 10<sup>2</sup>-fold) for targeting lymphatic vessels in mice using extremely low laser fluence levels. Antibody-conjugated GNTs were also used to bind to the lymphatic endothelial receptors in order to map the lymphatic endothelium, and preliminary *in vitro* viability tests showed that GNTs have minimal toxicity. More such approaches of combinatory imaging modalities are expected in the near future illustrating some of the advantages offered by CNTs.

**Table 12.1** Imaging modalities using CNT as contrast agents

<i>Imaging modality</i>	<i>Type of CNT</i>		<i>Source of signals</i>	<i>Preclinical animal model</i>	<i>In vivo/ex vivo</i>	<i>Conclusion</i>	<i>Ref.</i>
SPECT	Covalently modified CNTs by 1,3-dipolar cycloaddition	MWNT-NH <sub>3</sub> <sup>+</sup> chemically conjugated to DTPA	<sup>111</sup> In	Nude rats	<i>In vivo</i>	<i>Pros</i>	[20]
PET	Covalently modified CNTs by oxidation, 1,3-dipolar cycloaddition	SWNT-NH <sub>3</sub> <sup>+</sup> chemically conjugated to DOTA	<sup>86</sup> Y	Athymic nude mice	<i>In vivo</i>	<ul style="list-style-type: none"> <li>Clinically relevant</li> <li>High sensitivity (picomolar levels)/ medium resolution</li> </ul>	[24]
	Coated (noncovalently surface-modified) CNTs	pSWNT coated with PL-PEG-DOTA: SWNT-PEG2000-RGD SWNT-PEG2000 SWNT-PEG5400-RGD SWNT-PEG5400	<sup>64</sup> Cu	U87MG or HT-29 tumor-bearing nude mice	<i>In vivo</i>	<i>Cons</i> <ul style="list-style-type: none"> <li>Chemical modification of CNTs is required</li> <li>It detects the radiolabel, not the CNT, so stability of radiolabeling is critical</li> </ul>	[22]
Near IR-fluorescence	Coated (noncovalently surface-modified) CNTs	pSWNT coated with Pluronic F108	Intrinsic NIR fluorescence signals of SWNT	New Zealand rabbits	<i>Ex vivo</i>	<i>Pros</i>	[7]
		pSWNT coated with PL-PEG after lipid exchange with sodium cholate: exchange SWNT-PEG5000		LS174T tumor-bearing mouse	<i>In vivo</i>	<ul style="list-style-type: none"> <li>No chemical modification of SWNTs is required</li> </ul>	[36]
		direct SWNT-PEG5000			<i>Cons</i> <ul style="list-style-type: none"> <li>Restricted to individualized semimetallic SWNTs</li> <li>Low quantum efficiency of SWNT and the diffraction to resolution (medium sensitivity/ medium resolution)</li> <li>Poor tissue penetration</li> <li>Quantitative data are difficult to obtain using this technique.</li> </ul>		

<i>Imaging modality</i>	<i>Type of CNT</i>	<i>Source of signals</i>	<i>Preclinical animal model</i>	<i>In vivo/ex vivo</i>	<i>Conclusion</i>	<i>Ref.</i>	
Raman spectroscopy	Coated (noncovalently surface-modified) CNTs	pSWNT coated with PL-PEG-DOTA: SWNT-PEG2000-RGD SWNT-PEG2000 SWNT-PEG5400-RGD SWNT-PEG5400	Intrinsic Raman signals of SWNT	U87MG tumor-bearing nude mice	<i>Ex vivo</i>	<i>Pros</i>	[22]
		pSWNT coated with PL-PEG: SWNT-linear-PEG2000 SWNT-linear-PEG5000 SWNT-branched-PEG7000		Balb/c mice	<i>Ex vivo</i>	<ul style="list-style-type: none"> <li>Differentiates the spectral fingerprint of different particles allowing for multiplexing imaging</li> <li>Lack of background signals</li> <li>No labeling or encapsulation of Raman probes is required due to the inherent Raman signature of SWNT</li> <li>Raman signals are stable against photobleaching so suitable for long-term and repeated imaging weak signal intensity, which limits its sensitivity</li> </ul>	[23]
		pSWNT coated with chitosan or chitosan Alexa Fluor 488		Nude mice	<i>Ex vivo</i>	<i>Cons</i>	[16]
		pSWNT coated with PL-PEG: SWNT-PEG5000-RGD SWNT-PEG5000		U87MG tumor-bearing nude mice	<i>In vivo</i>	<ul style="list-style-type: none"> <li>Medium sensitivity/ poor resolution</li> <li>Poor signal (light) penetration (limited to below few centimeters of tissues)</li> <li>Laser source used to generate Raman signals can damage tissues</li> </ul>	[39]
MRI	Pristine CNTs	Raw SWNT Superpurified SWNT	Metal impurities inducing a drop in magnetic field homogeneity	Sprague-Dawley rats	<i>In vivo</i>	<i>Pros</i> <ul style="list-style-type: none"> <li>High resolution</li> <li>Good tissue penetration</li> </ul> <i>Cons</i> <ul style="list-style-type: none"> <li>Low sensitivity</li> </ul>	[1]

Imaging modality	Type of CNT	Source of signals	Preclinical animal model	In vivo/ex vivo	Conclusion	Ref.	
Photoacoustic tomography (PAT)	Coated (noncovalently surface-modified) CNTs	pSWNT coated with PL-PEG: SWNT-PEG5000-RGD SWNT-PEG5000	Intrinsic PA signals of SWNT	U87MG tumor-bearing nude mice	<i>In vivo</i>	Pros • Offers high spatial resolution (submillimeter)/medium sensitivity • Better tissue penetration than optical imaging techniques but still lower than nuclear imaging	[8]
		pSWNT dispersed in Pluronic F127	Intrinsic PA signals of SWNT	Sprague-Dawley rats	<i>In vivo</i>		[28]
	CNT coated with gold (GNT)	GNT with or without anti-LYVE-1 antibody	Intrinsic PA/PT signals of GNT	Murine mesentery with lymph node of Nu/nu mice	<i>In vivo</i>	Cons • Long acquisition time (20 min for single image of 100 mm <sup>3</sup> sized tumor)	[17]

## 12.3 CONCLUSIONS

The exploitation of CNTs in the biomedical arena has become an increasingly interesting area of research both at the basic biological level and also in the context of various therapeutic or diagnostic applications. The field has experienced an exponential increase in the number of studies and laboratories using CNTs in contact with various cells and tissues that will surely increase in the next few years. Several preclinical studies have been carried out to establish the suitability of CNT-based nanodevices as imaging contrast agents for small animal imaging *in vivo*. The sensitivity and resolution of these techniques varies; however, CNTs have also been shown to be successful candidates for multimodal imaging, i.e., using a combination of two or more imaging modalities. Such findings open a new era for the use of CNTs in multimodal imaging *in vivo*. Furthermore, CNTs have been shown to be able to carry therapeutic drug molecules in addition to contrast agents, thus allowing their use as theranostic devices. More work is required to optimize the sensitivity and to improve the biocompatibility of CNT-based devices to allow for smooth translation of these studies for clinical applications.

## References

1. Al-Faraj A., Cieslar K., Lacroix G., Gaillard S., Canet-Soulas E., and Cremillieux Y. (2009) *In vivo* imaging of carbon nanotube biodistribution using magnetic resonance imaging. *Nano Lett* **9**, 1023–1027.
2. Bhirde A. A., Patel V., Gavard J., Zhang G., Sousa A. A., Masedunskas A., Leapman R. D., Weigert R., Gutkind J. S., and Rusling J. F. (2009) Targeted killing of cancer cells *in vivo* and *in vitro* with EGF-directed carbon nanotube-based drug delivery. *ACS Nano* **3**, 307–316.
3. Bianco A. (2004) Carbon nanotubes for the delivery of therapeutic molecules. *Expert Opin Drug Deliv* **1**, 57–65.
4. Bianco A., Kostarelos K., Partidos C. D., and Prato M. (2005a) Biomedical applications of functionalised carbon nanotubes. *Chem Commun* 571–577.
5. Bianco A., Kostarelos K., and Prato M. (2005b) Applications of carbon nanotubes in drug delivery. *Curr Opin Chem Biol* **9**, 674–679.
6. Cai W., and Chen X. (2007) Nanoplatforms for targeted molecular imaging in living subjects. *Small* **3**, 1840–1854.
7. Cherukuri P., Gannon C. J., Leeuw T. K., Schmidt H. K., Smalley R. E., Curley S. A., and Weisman R. B. (2006) Mammalian pharmacokinetics of carbon nanotubes using intrinsic near-infrared fluorescence. *Proc Natl Acad Sci USA* **103**, 18882–18886.
8. De la Z. A., Zavaleta C., Keren S., Vaithilingam S., Bodapati S., Liu Z., Levi J., Smith B. R., Ma T. J., Oralkan O., Cheng Z., Chen X., Dai H., Khuri-Yakub B. T., and Gambhir S. S. (2008) Carbon nanotubes as photoacoustic molecular imaging agents in living mice. *Nat Nanotechnol* **3**, 557–562.
9. Ferrari M. (2005) Cancer nanotechnology: opportunities and challenges. *Nat Rev Cancer* **5**, 161–171.
10. Hirsch L. R., Gobin A. M., Lowery A. R., Tam F., Drezek R. A., Halas N. J., and West J. L. (2006) Metal nanoshells. *Ann Biomed Eng* **34**, 15–22.
11. Huh Y., Shao L., Tobias G., Green M. L. (2006) Opening and reversible filling of single-walled carbon nanotubes with various materials. *J Nanosci Nanotechnol* **6**, 3360–3363.
12. Iijima S. (1996) Structural flexibility of carbon nanotubes. *J Jap Soc Tribol* **41**, 724–729.
13. Kam N. W., Liu Z., and Dai H. (2005a) Functionalization of carbon nanotubes via cleavable disulfide bonds for efficient intracellular delivery of siRNA and potent gene silencing. *J Am Chem Soc* **127**, 12492–12493.
14. Kam N. W., Liu Z., Dai H. (2006) Carbon nanotubes as intracellular transporters for proteins and DNA: an investigation of the uptake mechanism and pathway. *Angew Chem Int Ed Engl* **45**, 577–581.
15. Kam N. W., O'Connell M., Wisdom J. A., and Dai H. (2005b) Carbon nanotubes as multifunctional biological transporters and near-infrared agents for selective cancer cell destruction. *Proc Natl Acad Sci USA* **102**, 11600–11605.
16. Kang B., Yu D., Dai Y., Chang S., Chen D., and Ding Y. (2009) Biodistribution and

- accumulation of intravenously administered carbon nanotubes in mice probed by Raman spectroscopy and fluorescent labeling. *Carbon* **47**, 1189–1206.
17. Kim J. W., Galanzha E. I., Shashkov E. V., Moon H. M., and Zharov V. P. (2009) Golden carbon nanotubes as multimodal photoacoustic and photothermal high-contrast molecular agents. *Nat Nanotechnol* **4**, 688–694.
  18. Kostarelos K., Bianco A., and Prato M. (2009) Promises, facts and challenges for carbon nanotubes in imaging and therapeutics. *Nat Nanotechnol* **4**, 627–633.
  19. Lacerda L., Bianco A., Prato M., and Kostarelos K. (2006) Carbon nanotubes as nanomedicines: From toxicology to pharmacology. *Adv Drug Delivery Rev* **58**, 1460–1470.
  20. Lacerda L., Soundararajan A., Singh R., Pastorin G., Al-Jamal K. T., Turton J., Frederik P., Herrero M. A., Bao S. L. A., Emfietzoglou D., Mather S., Phillips W. T., Prato M., Bianco A., Goins B., and Kostarelos K. (2008) Dynamic Imaging of functionalized multi-walled carbon nanotube systemic circulation and urinary excretion. *Adv Mater* **20**, 225–230.
  21. Li Z. B., Cai W., and Chen X. (2007) Semiconductor quantum dots for *in vivo* imaging. *J Nanosci Nanotechnol* **7**, 2567–2581.
  22. Liu Z., Cai W., He L., Nakayama N., Chen K., Sun X., Chen X., and Dai H. (2007) *In vivo* biodistribution and highly efficient tumour targeting of carbon nanotubes in mice. *Nat Nanotechnol* **2**, 47–52.
  23. Liu Z., Davis C., Cai W. B., He L., Chen X. Y., and Dai H. J. (2008) Circulation and long-term fate of functionalized, biocompatible single-walled carbon nanotubes in mice probed by Raman spectroscopy. *Proc Natl Acad Sci USA* **105**, 1410–1415.
  24. McDevitt M. R., Chattopadhyay D., Jaggi J. S., Finn R. D., Zanzonico P. B., Villa C., Rey D., Mendenhall J., Batt C. A., Njardarson J. T., Scheinberg D. A. (2007a) PET imaging of soluble yttrium-86-labeled carbon nanotubes in mice. *PLoS ONE* **2**, e907.
  25. McDevitt M. R., Chattopadhyay D., Kappel B. J., Jaggi J. S., Schiffman S. R., Antczak C., Njardarson J. T., Brentjens R., and Scheinberg D. A. (2007b) Tumor targeting with antibody-functionalized, radiolabeled carbon nanotubes. *J Nucl Med* **48**, 1180–1189.
  26. Pastorin G., Wu W., Wieckowski S., Briand J. P., Kostarelos K., Prato M., and Bianco A. (2006) Double functionalization of carbon nanotubes for multimodal drug delivery. *Chem Commun (Camb)* 1182–1184.
  27. Podesta J. E., Al-Jamal K. T., Herrero M. A., Tian B., li-Boucetta H., Hegde V., Bianco A., Prato M., and Kostarelos K. (2009) Antitumor activity and prolonged survival by carbon-nanotube-mediated therapeutic siRNA silencing in a human lung xenograft model. *Small* **5**, 1176–1185.
  28. Pramanik M., Song K. H., Swierczewska M., Green D., Sitharaman B., and Wang L. V. (2009a) *In vivo* carbon nanotube-enhanced noninvasive photoacoustic mapping of the sentinel lymph node. *Phys Med Biol* **54**, 3291–3301.
  29. Pramanik M., Swierczewska M., Green D., Sitharaman B., and Wang L. V. (2009b) Single-walled carbon nanotubes as a multimodal-thermoacoustic and photoacoustic-contrast agent. *J Biomed Opt* **14**, 034018.

30. Shao L., Lin T. W., Tobias G., and Green M. L. (2008) A simple method for the containment and purification of filled open-ended single wall carbon nanotubes using C60 molecules. *Chem Commun (Camb)* 2164–2166.
31. Singh R., Pantarotto D., Lacerda L., Pastorin G., Klumpp C., Prato M., Bianco A., and Kostarelos K. (2006) Tissue biodistribution and blood clearance rates of intravenously administered carbon nanotube radiotracers. *Proc Natl Acad Sci USA* **103**, 3357–3362.
32. Singh R., Pantarotto D., McCarthy D., Chaloin O., Hoebeke J., Partidos C. D., Briand J. P., Prato M., Bianco A., and Kostarelos K. (2005) Binding and condensation of plasmid DNA onto functionalized carbon nanotubes: toward the construction of nanotube-based gene delivery vectors. *J Am Chem Soc* **127**, 4388–4396.
33. Sitharaman B., Kissell K. R., Hartman K. B., Tran L. A., Baikalov A., Rusakova I., Sun Y., Khant H. A., Ludtke S. J., Chiu W., Laus S., Toth E., Helm L., Merbach A. E., and Wilson L. J. (2005) Superparamagnetic gadonanotubes are high-performance MRI contrast agents. *Chem Commun (Camb)*, 3915–3917.
34. Thorek D. L., Chen A. K., Czupryna J., and Tsourkas A. (2006) Superparamagnetic iron oxide nanoparticle probes for molecular imaging. *Ann Biomed Eng* **34**, 23–38.
35. Tilmaciu C. M., Soula B., Galibert A. M., Lukanov P., Datas L., Gonzalez J., Barquin L. F., Rodriguez F. J., Gonzalez-Jimenez F., Jorge J., and Flahaut E. (2009) Synthesis of superparamagnetic iron(III) oxide nanowires in double-walled carbon nanotubes. *Chem Commun (Camb)* 6664–6666.
36. Welsher K., Liu Z., Sherlock S. P., Robinson J. T., Chen Z., Daranciang D., and Dai H. (2009) A route to brightly fluorescent carbon nanotubes for near-infrared imaging in mice. *Nat Nanotechnol* **4**, 773–780.
37. Wu W., Wieckowski S., Pastorin G., Benincasa M., Klumpp C., Briand J. P., Gennaro R., Prato M., and Bianco A. (2005) Targeted delivery of amphotericin B to cells by using functionalized carbon nanotubes. *Angew Chem Int Ed Engl* **44**, 6358–6362.
38. Yang S. T., Wang H., Mezziani M. J., Liu Y., Wang X., and Sun Y. P. (2009) Biodefunctionalization of functionalized single-walled carbon nanotubes in mice. *Biomacromolecules* **10**, 2009–2012.
39. Zavaleta C., De la Z. A., Liu Z., Keren S., Cheng Z., Schipper M., Chen X., Dai H., and Gambhir S. S. (2008) Noninvasive Raman spectroscopy in living mice for evaluation of tumor targeting with carbon nanotubes. *Nano Lett* **8**, 2800–2805.
40. Zhang Z., Yang X., Zhang Y., Zeng B., Wang S., Zhu T., Roden R. B., Chen Y., and Yang R. (2006) Delivery of telomerase reverse transcriptase small interfering RNA in complex with positively charged single-walled carbon nanotubes suppresses tumor growth. *Clin Cancer Res* **12**, 4933–4939.

